# A theoretical study on the P-I diagram of framed monolithic glass window subjected to blast loading

**Citation for published version:**
Chen, S, Chen, X, Li, G & Lu, Y 2017, 'A theoretical study on the P-I diagram of framed monolithic glass window subjected to blast loading', *Engineering Structures*, vol. 150, pp. 497-510.
https://doi.org/10.1016/j.engstruct.2017.07.055

**Digital Object Identifier (DOI):**
10.1016/j.engstruct.2017.07.055



**Published In:**
Engineering Structures

# A Theoretical Study on the P-I Diagram of Framed Monolithic Glass Window Subjected to Blast Loading

Suwen CHEN [1,2], Xing CHEN [2], Guo-Qiang LI [1,2], Yong LU [3]

[1] State Key Laboratory for Disaster Reduction in Civil Engineering, Tongji University, Shanghai 200092, China

[2] College of Civil Engineering, Tongji University, Shanghai 200092, China

[3] Institute for Infrastructure and Environment, School of Engineering, The University of Edinburgh, Edinburgh EH9 3JL, UK

ABSTRACT

In this paper, an analytical model for determining the iso-damage curves for framed monolithic glass panels subjected to blast loading is proposed. Two typical damage levels corresponding to different conditions in GSA/ISC are classified, namely a) the glass crack limit and b) glass fragments invading with a certain velocity. The nonlinear dynamic responses and failure modes of framed monolithic glass under different blast loadings are firstly analysed numerically. Then critical states of glass panel in both impulsive region and quasi-static region of the pressure-impulse (P-I) diagram are defined. Based on the energy balance approach, an analytical method is proposed for determining the pressure asymptote and the impulse asymptote of framed monolithic glass for different damage levels. The proposed method is verified through comparison with published experimental data and numerical results. The method can be applied for any framed monolithic glazing with different dimension and thickness and provides a practical approach for engineering design and hazard level estimation of framed monolithic glass against blast loading.

**Keywords:** Framed glass window; Monolithic glass; blast loading, P-I diagram; failure modes; analytical method

## NOMENCLATURE

| | |
|---|---|
| $a$, $b$ | length and width of the monolithic glass panel, with $a \geq b$ |
| $h$ | thickness of the monolithic glass panel |
| $E$ | elastic modulus of glass |
| $G$ | shear modulus of glass |
| $v$ | Poisson's ratio of glass |
| $\sigma_f$ | failure stress of glass material |
| $\psi$ | deflection function of glass panel |
| $w$ | deflection at the panel centre |
| $w_f$ | deflection at the panel centre at glass crack moment |
| $p$ | peak overpressure of a specific blast load |
| $i$ | impulse of positive phase of a specific blast load |
| $t_d$ | equivalent positive load duration of a specific blast load |
| $D_s$ | width of shear region |
| $C$ | length of shear region |
| $M_e$ | equivalent mass of the equivalent model |
| $K_b$, $K_s$ | flexural stiffness and shear stiffness of the equivalent model |
| $K_e$ | effective stiffness of the equivalent model |
| $P_e$ | equivalent load of the equivalent model |
| $W$ | the work done by the pressure |
| $\Delta_b$, $\Delta_s$ | flexural deflection and shear deflection of the equivalent model |
| $\Delta$ | effective deflection of the equivalent model |
| $\sigma_1$ | maximum principal stress within the glass panel |
| $E_{k0}$ | initial kinetic energy of glass panel |
| $E_k$ | total kinetic energy of glass panel |
| $E_{kr}$ | residual kinetic energy at glass failure moment |
| $v_0$ | initial velocity at the panel centre |
| $v_r$ | ejection velocity of the glass fragments |
| $U_i$ | internal strain energy of the panel |
| $U_f$ | dissipated energy due to glass fracture |
| $\gamma_s$ | surface energy per unit area |
| $\Delta a$ | side length of a representative square fragment |
| $A_f$ | area of new formed surfaces of fragments |
| $i_{cr}^k$, $p_{cr}^k$ | values of impulse asymptote and overpressure asymptote for damage level $k$, respectively. $k$=I,II,III… |
| $\alpha$, $\beta$ | shape parameter for the dynamic region of P-I curve |
| $\xi$ | adjust coefficient to modify the impulse asymptote of damage level I |
| $i_c^1$ | modified impulse asymptote of damage level I |
| $T_s$ | natural period of glass panel |
| $\lambda$ | ratio of residual kinetic energy to total energy at glass failure moment |
| $\lambda_c$ | critical residual kinetic energy ratio for punching failure mode |
| $v_{rc}$ | critical ejection velocity for punching failure mode |
| $D_{sc}$ | shearing region width for critical damage level |

## 1. INTRODUCTION

Glass curtain wall has become more and more popular in high-rise buildings nowadays for its artistic facade appearance and high clarity. However, its disadvantages are also very significant. Because glass is a brittle material with relatively weak strength compared with other structural members, glazing windows are more vulnerable to air blast waves caused by intentional or accidental explosions. Laminated glass has been proved to be very effective at mitigating the risk of fragment ejection, and therefore it is widely used and should be a priority choice in regions where high level of protection is required. However, due to the un-predictable nature of explosion occurrence, especially for concerns over malicious attacks, it is necessary to investigate monolithic glass as it is still the most commonly used glass type in the general building stock. According to the statistical data in literature [1], as listed in Table 1, over 40% of the injuries in an explosion incident have been glass-related injuries such as lacerations and abrasions from flying glass shards. Therefore, it is very important to strive for a proper design of glass windows with consideration of possible exposure to blast loading, and to this end a thorough understanding of the dynamic behaviour and failure mechanism of glass windows subjected to blast wave is crucial.

GSA/ISC [2] classifies the performance of window systems subjected to blast loads and the related hazard levels, as indicated in Figure 1. These response conditions are classified based upon the post-test location of fragments and debris. Under condition 1 or 2 there will be little fragments invade and the glazing remains to be retained by the frame. Only dusting or very small fragments near the sill or on the floor may be acceptable. Condition 3a to 5 are specified according to the invasion distance and the corresponding hazard level. For example, condition 3a and 3b correspond to invasion distances of no more than 1m and 3m respectively, while condition 4 or 5 represent fragments that can impact a target located 3m away from the window at a height lower or higher than 0.6m above the floor, respectively. Currently, for design of blast resistant glazing, ASTM-F2248 and ASTM-E1300 [3, 4] specify an equivalent 3-second duration design loading and design charts for different types of glass windows. However, neither the dynamic characteristics of the blast loading nor the dynamic response of glazing has been considered in these ASTM standards [3, 4]. Besides, it should be noted that the equivalent 3-second duration uniform load is associated with a probability of breakage less than or equal to 8 lites per 1000 for monolithic annealed glass, which cannot satisfy the demand of multi damage level based design.

This paper is concerned with the development of iso-damage curves for different damage levels of framed monolithic glass subjected to blast loading, which is to be used for practical applications in the blast resistant design of glazing as well as hazard estimation. A lot of research, including analytical derivation, field blast test and numerical simulation has been devoted to establish the iso-damage curves for glass windows. In particular, many studies have been conducted to predict the response of glass panel using a single-degree-of-freedom (SDOF) approach [5-7]. Cormie et al [7] developed a theoretical method to describe the behaviour of laminated glass, and proposed iso-damage curves for laminated glass under blast loading using a SDOF model. These iso-damage curves were compared with FEA results by Hooper [8] and Zhang [9], and the results revealed considerable errors in the values of impulse asymptote under different damage levels. The insufficient accuracy in the existing SDOF method for predicting blast resistant capacity of glass panels in different response regimes is believed to stem from the fact that the deformation shape function is inaccurate under impulsive loading.

On the other hand, experimental investigations including field blast tests and shock tube tests have also been conducted [10-16], most of which, however, were restricted to specific window sizes and material properties. As it is very expensive to conduct blast tests, it is not practical to rely on large numbers of blast tests to parametrically study the performance of glass panels or to obtain the detailed P-I curves. Numerical parametric study is another way to establish P-I curves. But the results based on numerical study and blast tests are only applicable to specific dimensions and thicknesses, therefore is not generally applicable. To achieve generality, developing a physics-based theoretical method for establishing P-I curves becomes of indispensable value.

In this paper, a theoretical method is proposed for establishing the iso-damage curves for framed monolithic glass for different damage levels, which can be applied to any fixed framed monolithic glazing with variable dimensions and thicknesses. Firstly, two typical damage levels corresponding to different conditions in GSA/ISC [2] are classified, namely a) the glass crack limit and b) glass fragment invading with a certain velocity. The nonlinear dynamic responses and failure modes of framed monolithic glass under different blast loadings are analysed by means of finite element method. Then, critical states of glass panel in both impulsive region and quasi-static region of the pressure-impulse (P-I) diagram for different damage levels are defined. Based on the energy balance approach, the analytical method for calculating the pressure asymptote and the impulse asymptote of framed monolithic glass for different damage levels are proposed. The proposed method is verified through comparison with published experimental data and numerical simulation results. The method is shown to provide reliable prediction of the pressure-impulse (P-I) diagram of framed monolithic glass panel for different damage levels, and it can be used for quick estimation of splashing distance for an existing design and assess the hazard level, or a new design with a required hazard level.

## 2. DESCRIPTION OF P-I CURVE

According to previous study, a P-I curve for a certain structure may be expressed by the following

Equation [9, 17]:

$$(p - p_{cr}^{k})(i - i_{cr}^{k}) = \alpha\left(\frac{p_{cr}^{k}}{2} + \frac{i_{cr}^{k}}{2}\right)^{\beta} \quad (1)$$

where $p$ is the peak overpressure, $i$ is the impulse, $i_{cr}^{k}$ denotes the impulse value of the impulsive asymptote for a given damage level $k$, $p_{cr}^{k}$ is the overpressure value of the overpressure asymptote for the same failure level; α and β are parameters related to the properties of the structure, which determine the shape of the curve in the dynamic zone, as shown in Figure 4.

A blast load with a peak overpressure and an impulse above a P-I curve will result in the corresponding damage level of the structure, whereas the structure will be safe or undergo lesser damage if the peak overpressure and impulse combination is located below or left to the curve. In the following section, $i_{cr}^{k}$ and $p_{cr}^{k}$ are calculated employing energy method, and the deflection functions are determined based on the failure modes in the impulse zone and the quasi-static zone respectively. Due to the complexity of failure mode in the dynamic zone, it is very difficult to figure out an analytical solution for the shape parameters (α and β). Therefore a series of numerical test points are generated for the dynamic zone of the P-I curve to determine numerically the shape parameters for different damage levels.

In this paper, three typical damage levels are defined to satisfy different blast resistant design requirements, as listed in Table 2. Damage level I represents the onset of crack of glass corresponding to condition 2 in GSA/ISC [2] (Figure 1). Damage level II and III represent the glass fragment invading with a certain velocity, which corresponds to condition 3a to 5 in GSA/ISC [2] (Figure 1).

## 3. ANALYTICAL MODEL

In the analytical model， a typical glass panel with dimensions of $a \times b \times h$ ($a \geq b$) is assumed to be gripped within an steel frame (Figure 2), in which $a$, $b$ and $h$ represent the length, width and thickness of the glass panel respectively. The boundary condition for the glass panel is simplified as fixed due to the constraint of the frame. The blast load is simplified as a triangular decay uniform pressure that acts perpendicularly to the glass panel.

In a typical blast load scenario, the blast overpressure rapidly rises to the peak positive pressure, then it gradually reduces until it reaches the peak negative pressure, and finally it picks up to the ambient pressure slowly, as is shown in Figure 3. Previous study shows that negative phase may have a significant influence on cases where the rebound occurs during the negative phase [18, 19], and pull-out failure may take place due to the combination of elastic recovery force and the negative phase of loading. The main purpose of the present study is to propose a theoretical model for impulse asymptote and overpressure asymptote of P-I curves, where the corresponding $t_d/T$ ratio (in which $t_d$ is the load duration and T is the natural period of the panel) is less than 0.1 or larger than 10 [7]. It has been indicated that the effect of negative phase is insignificant in both ranges [18], so in the present study the negative phase is ignored and a triangular decay function is adopted to describe the blast loading for simplification. Therefore, the main parameters of the blast load are peak overpressure and positive phase duration. In the case of explosion in a close range, the blast loading has very high overpressure but very short duration, which is a characteristic of impulsive loading. In long-range blast cases, the overpressure decreases relatively slowly, resulting in long loading duration and hence a “quasi-static” type of loading. The coordinates on a pressure-impulse (P-I) plot can well represent the characteristics of the blast load, and therefore with the P-I curve the bearing capacity of glass panel subjected to different blast loadings can be well expressed. It should also be noted that the uniform blast pressure assumption is only valid when the explosion is not very close to the glass panel. This is actually the general condition the current study is focused on; otherwise non-uniform blast loading distribution has to be considered due to different blast shock wave propagation distances and incident angles. As a matter of fact, very-close range explosion may lead to the destruction of structural members, in which case the failure of glazing is not a primary concern. Therefore a uniform blast pressure is considered suitable for general analysis of glass panels in the present study. Further study is needed to investigate the failure mechanism of glass panel subjected to very close explosion.

## 3.1 SOLUTION OF THE OVERPRESSURE ASYMPTOTE

The overpressure asymptote reflects the bearing capacity of a glass panel in the quasi-static region. In this region, the deflection of a four-side-fixed glass panel can be assumed to follow the classical slab deflection and expressed as [20]

$$\psi(x,y)=\cos^2(\frac{\pi x}{a})\cos^2(\frac{\pi y}{b})\,,\quad -\frac{a}{2}\le x\le\frac{a}{2}\,,\quad -\frac{b}{2}\le y\le\frac{b}{2} \tag{2}$$

Based on the assumed shape function $\psi(x,y)$, an equivalent SDOF system can be built and the corresponding parameters can be obtained as follows [21]:

$$M_e=\iint m\psi^2(x,y)dxdy \tag{3}$$

$$K_e=\iint\frac{Et^3}{12(1-v^2)}\left\{\left[\frac{\partial^2\psi(x,y)}{\partial x^2}+\frac{\partial^2\psi(x,y)}{\partial y^2}\right]^2-2(1-v)\left[\frac{\partial^2\psi(x,y)}{\partial x^2}\frac{\partial^2\psi(x,y)}{\partial y^2}-\frac{\partial^2\psi(x,y)}{\partial x\partial y}\right]\right\}dxdy \tag{4}$$

$$P_e=\iint p_0\psi(x,y)dxdy \tag{5}$$

where $M_e$, $K_e$ and $P_e$ are the equivalent mass, equivalent stiffness and equivalent load of the SDOF system respectively. $m$ is the mass of glass panel per unit area, and $p_0$ is the uniform overpressure acting on the glass panel. $E$ and $v$ are the elastic modulus and Poisson's ratio of glass respectively.

Based on the small-deflection theory of bending, the stresses in the glass panel can be calculated using the stress-strain relations. The maximum stress occurs at the panel centre, which is also the maximum principal stress ($\sigma_1$) within the glass panel, as follows:

$$\sigma_1 = w \cdot \frac{Eh\pi^2}{2(1-v^2)} \frac{(a^2+vb^2)}{a^2b^2} \tag{6}$$

where $w$ is the displacement at panel centre.

By equalling the maximum principal stress $\sigma_1$ to the failure strength of glass $\sigma_f$, the failure displacement $w_f$ can be obtained as follows:

$$w_f = \sigma_f \cdot \frac{1-v^2}{Eh\pi^2} \frac{a^2b^2}{(a^2+vb^2)} \tag{7}$$

It should be mentioned that glass failure is very sensitive to initial micro cracks and is therefore probability-dependent. In practical engineering design, the failure probability of the strength of glass is considered by introducing a strength reduction coefficient, and the corresponding design strength is given for different glass types and thicknesses [22]. When applying the method proposed in this study for design analysis, the failure strength can either be taken as the design value from relevant design codes, so that the probability-dependent failure is represented in a code-compatible manner, or be determined based on material test results.

In the quasi-static region, the applied pressure is considered to be constant in time, so the work done by the pressure, $W$, can be calculated as:

$$W = P_e \cdot w_f \tag{8}$$

Based on the SDOF method [21], the internal strain energy $U_i$ and residual kinetic energy $E_{kr}$ are given by Equation 7 and Equation 8, respectively:

$$U_i = \frac{1}{2} K_e w_f^2 \tag{9}$$

$$E_{kr} = \frac{1}{2} M_e v_r^2 \tag{10}$$

where $v_r$ represents the ejection velocity.

For damage level I, which represents the onset of glass cracking, there is no residual kinetic energy or fracture energy, which means $E_{kr}$ and $U_f$ equal 0. Thus the external work $W$ will transform into the strain energy corresponding to the limit strain of cracking, $U_i$.

For damage level II, $W$ will transform into strain energy corresponding to the limit strain of cracking $U_i$, residual kinetic energy $E_{kr}$, and the energy dissipated by glass fracture $U_f$ :

$$W = U_i + E_{kr} + U_f \tag{11}$$

$E_{kr}$ may be evaluated according to a specific ejection velocity through Equation 10. The determination of dissipated energy $U_f$ will be detailed in Section 3.3.

Once we obtain the external work $W$, the corresponding external pressure $p_{cr}^k$, which defines the value of the overpressure asymptote, can be determined by:

$$p_{cr}^k = \frac{W}{w_f \cdot \iint \psi(x,y) dxdy} \tag{12}$$

## 3.2 Theoretical Model for Impulsive Region

When the loading duration is very short, the response will depend on impulse rather than the peak load. For example if we assume a triangle pulse shape, then according to the structural dynamics theory the impulsive response will occur if the ratio between the duration of the loading and the natural period of the system ($t_d/T$) is less than 0.1 [7].

It is generally known that three failure modes could take place under impulsive loading, namely flexural failure, shear failure, and a combination of the two modes. A typical four-side-fixed monolithic panel in size of 1100mm×1100mm×8mm is modelled here to illustrate how the failure mode changes with different imposed impulse, as shown in Figure 5. The detailed finite element (FE) model will be described later in Section 3. It should be noted that the peak overpressure considered in blast resistance design for glazing is relatively smaller comparing with those for main structural members, and therefore in current study a peak overpressure not exceeding 2000kpa is considered for impulsive loading in numerical analysis.

As can be seen from Figure 5, when the impulse is just above the critical limit (impulse asymptote) of damage level I (glass crack limit), the failure mode of the laminated glass is of a flexure pattern, with the cracks mainly occurring around the centre of glass panel as a result of bending deformation.

When the impulse is much larger than the impulse asymptote value for glass crack limit, the damage of the glass panel tends to initiate earlier and at locations near the boundary, giving rise to a clear punching-type shear failure mode. In-between the above two modes, mixed patterns of cracks occur, indicating a combination of flexural failure and shear failure.

Figure 6 shows a typical development of the deflection profiles obtained by FEA for a fixed glass panel under impulsive loading, and the applied blast loading (p=2000kPa and i=24kPa·ms) is very close to impulse asymptote for damage level I. As can be seen, because the impulse is not large enough to cause a punching-type of shear failure at the early stage of the response, the panel will enter into the stage of global bending deformation and results in flexural failure; in the particular example herein this occurs at t=3.4ms. This gives the critical state of glass panel along the impulse asymptote of damage level I.

Because of the global bending nature of the critical failure mode, the deflection mode of the fixed glass panel along the impulse asymptote of damage level I can be assumed the same as that of the quasi-static region. Figure 7 shows a comparison of the deflections obtained by FEA at a global bending failure under an impulsive load and that of theoretical hypothesis (i.e. deflection under a quasi-static load), giving a good agreement. The strain energy $U_i$ required for this critical failure mode to develop under an impulsive load can be obtained by Equation 9 as well.

For the quantification of the impulsive load, it is convenient to consider it to be a pure impulse *i*. Assuming a triangle pulse shape,

$$i = \frac{1}{2} p t_d \tag{13}$$

where $p$ and $t_d$ are the peak overpressure and equivalent positive load duration of a specific blast load respectively.

From impulse – momentum transfer, the initial velocity at the panel centre $v_0$ can be written as

$$v_0 = \frac{iab}{M_e} \tag{14}$$

where *iab* equals to the total impulse calculated over the slab, $M_e$ is the effective mass.

Accordingly the initial kinetic energy of the system will be:

$$E_{k0} = \frac{1}{2} M_e v_0^2 \tag{15}$$

For damage level I which corresponds to the onset of glass crack, the initial kinetic energy $E_{k0}$ will completely transform into strain energy $U_i$ at glass failure moment. In other words there will be no residual kinetic energy after glass fracture, or the imposed loading would be larger than the critical loading corresponding to glass crack limit. Thus, the energy transformation relationship can be written as

$$E_{k0} = U_i \tag{16}$$

This gives rise to the required minimum explosion impulse for the damage level I:

$$i_{cr}^{I} = \frac{1}{ab} \sqrt{2 M_e U_i} \tag{17}$$

When it comes to damage level II, where the impulse is large enough, damage can develop in a very rapid manner prior to the development of a flexural deformation mode and flexural failure. The failure of glass panel is therefore mainly caused by the shearing force near the boundaries, as has been explained earlier and shown in Figure 5. The whole panel will detach from the frame after the cracks linking up along the boundary, indicating a punching failure. In this case, only a fraction of the impact energy is dissipated by local fracture while the remaining part exists as kinetic energy, consequently leading to the high speed flying fragments. Figure 8 shows the contours of displacement and stress of glass panel under impulsive loading for level II obtained by FEA. In the early phase, the deformation and stress level in the core region is negligible as compared with those in the shearing region. The damage zone forms an annular shape along the glass boundaries with a width of $D_s$, as depicted in Figure 8 and 9.

In order to describe the dynamic behaviour of the glass panel in such a concentrated zone, herein we propose a simplified short beam model, as shown in Figure 10. The boundary condition in the model is simplified as clamped such that there is no rotation at the two ends of the beam. This assumption is deemed reasonable concerning the shear failure mode as described earlier. The length of the beam equals the width of the shear region $D_s$ while the cumulative “width” of the beam equals the circumference of the shearing region $C$,

$$C = 2(a + b - 2D_s) \tag{18}$$

In the simplified beam model, the bending stiffness and shearing stiffness are given by Equation 19 and 20,

$$K_b = \frac{12EI}{D_s^3} \tag{19}$$

$$K_s = \frac{GA}{D_s} \tag{20}$$

where $E$ and $G$ are the elastic modulus and shear modulus respectively, $A$ is the section area which equals $C \times h$, $I$ is the section inertia which equals $Ch^3/12$, and $h$ is the depth of the panel.

The rigid movement of core region can then be represented by the deformation at the end of the beam $\Delta$, which is combined of the shearing deformation $\Delta_s$ and bending deformation $\Delta_b$,

$$\Delta = \Delta_s + \Delta_b \tag{21}$$

According to the deformation-stiffness relationship, the following effective stiffness $K_e$ is obtained:

$$K_e = \frac{K_s K_b}{K_b + K_s} \tag{22}$$

The displacement caused by shearing deformation and bending deformation can also be separated from total displacement, as follows:

$$\Delta_s = \Delta \cdot \frac{K_e}{K_s} \tag{23}$$

$$\Delta_b = \Delta \cdot \frac{K_e}{K_b} \tag{24}$$

Consequently the bending moment $M$ and shear force $F_s$ applied at the ends of the beam can be obtained as:

$$M = K_b \cdot \Delta_b \cdot \frac{D_s}{2} \tag{25}$$

$$F_s = K_s \cdot \Delta_s \tag{26}$$

By equating the maximum bending stress $\sigma_m$ to the failure stress of glass $\sigma_f$ (Equation 27) the failure displacement controlled by bending effect is given Equation 28.

$$\sigma_m = \frac{M}{I} \cdot \frac{h}{2} = \sigma_f \tag{27}$$

$$w_{f1} = \frac{Ch^2 \sigma_f}{3K_e D_s} \tag{28}$$

On the other hand, by equating the maximum principal stress $\sigma_1$, which equals $\tau_\mathrm{m}$ under a pure shear condition, to the failure stress of glass $\sigma_f$ (Equation 29), the failure displacement controlled by shearing stress can then be determined by Equation 30.

$$\sigma_1 = \tau_m = \frac{3F_s}{2A} = \sigma_f \tag{29}$$

$$w_{f2} = \frac{2Ch\sigma_f}{3K_e} \tag{30}$$

The actual failure displacement is the smaller between the bending controlled displacement and shearing controlled displacement,

$$w_f = \min[w_{f1}, w_{f2}] \tag{31}$$

Therefore the bending deformation $\Delta_{bf}$ and shearing deformation $\Delta_{sf}$ at failure moment can be given by:

$$\Delta_{sf} = w_f \cdot \frac{K_e}{K_s} \tag{32}$$

$$\Delta_{bf} = w_f \cdot \frac{K_e}{K_b} \tag{33}$$

The bending strain energy and shearing strain energy of the glass panel when failure occurs are obtained by Equation 34 and 35. The total energy of glass panel is the combination of bending strain energy and shearing strain energy, which is given by Equation 36.

$$U_b = \int_0^{D_s} \frac{M^2(x)}{2EI} dx = \frac{6EI}{D_s^3} \cdot \Delta_{bf}^2 \tag{34}$$

$$U_s = \int_0^{D_s} \frac{V^2(x)}{2GA} dx = \frac{GA}{2D_s} \cdot \Delta_{sf}^2 \tag{35}$$

$$U_i = U_b + U_s \tag{36}$$

The initial kinetic energy imparted by explosion impulse has been given by Equation 15. Based on energy conservation, the initial kinetic energy $E_{k0}$ will transform into the strain energy in the concentrated deformed band (i.e. the "beam") $U_i$, the residual kinetic energy of the panel $E_{kr}$ , and the fracture energy for the central panel region $U_f$, as shown in Equation 37. $E_{kr}$ may be evaluated according to specific ejection velocity of fragments. Thus the blast load impulse can be calculated by Equation 38, which represents the value of $i_{cr}^{II}$.

$$\frac{I_0^2}{2M_e} = E_{k0} = U_i + E_{kr} + U_f \tag{37}$$

$$i_{cr}^{II} = \frac{1}{ab}\sqrt{2M_e(U_i + E_{kr} + U_f)} \tag{38}$$

3.3 Determination of the Fracture Energy of the Glass Panel

In the above section the strain energy stored in the concentrated "beam" zone up to glass fracture has been formulated for the impulsive regime. The main panel is simplified as rigid body, however in reality the whole glass panel will be involved in the fragmentation process once the fracture limit is reached. From the energy point of view, the breakup of the central area of the panel will require additional input energy for the formation of new fragment surfaces [23, 24]. Based on the Griffith energy balance criterion [25], the fragmentation energy may be written as

$$U_f = A_f \gamma_s \tag{39}$$

where $A_f$ is the total surface area of fracture and $\gamma_s$ is the surface energy per unit area. For the monolithic glass plate, $\gamma_s$ is 3.9 J/m$^2$ for soda-lime glass in static state [24].

To simplify the calculations, a representative square fragment with a side length of $\Delta a$ is taken as an example, as shown in Figure 11, and therefore the total amount of fragments can be obtained as $\frac{ab}{\Delta a^2}$. Then the area of new formed surfaces equals the total surface area of fragments minus the original surface area of glass panel, which can be written as

$$A_f = \frac{ab}{\Delta a^2} \times (4\Delta ah + 2\Delta a^2) - 2ah - 2bh - 2ab \tag{40}$$

Substituting Equation 40 into Equation 39, the total fragmentation energy of the panel for a given fragment size ( $\Delta a$ ) is given by

$$U_f = 2h(\frac{2ab}{\Delta a} - a - b)\gamma_s \tag{41}$$

Previous experimental investigations show that the glass fragment characteristic is affected by many factors, including panel sizes, blast loading conditions (strain rate) and glass types et al. [12, 26, 27]. For example, in Zhang's test [27], the nominal length (square root of the measured fragment area) of fragment mainly varies between 15mm to 80mm for each load case, and fragments with nominal length less than 30mm shows a dominant proportion. Besides, the amount of small fragments increases as the reflected pressure and impulse increases. Here two extreme cases are considered here to analyze the influence of different fragment sizes on the calculation results, in which the fragment sizes are taken as 15mm and 80mm respectively. According to Equation 41, the resulting surface energy for a 1500mm×1200mm×10mm is 2.13J and 18.51J respectively. If the ejection velocity is assumed as 5m/s, the corresponding kinetic energy will be 441.1J based on Equation 10, which is more than 20 times the magnitude of surface energy. Then it can be concluded that surface energy is relatively small comparing with the kinetic energy of flying fragment and its influence on calculation results is negligible. Due to the glass size is very difficult to be determined for various glass panels and load cases, a constant fragment size of 20mm is utilised in the present study for an easy estimation of the surface energy. Accordingly, the dissipated energy due to glass fracture can be obtained based on Equation 39 and 41.

## 4. NUMERICAL STUDY

As discussed in Section 2, the shape parameters ($\alpha$ and $\beta$) of the P-I curves are determined through a numerical simulation study instead of using a theoretical approach due to the complexity of failure mode in the dynamic zone of the P-I curves. In this section, numerical analysis for framed monolithic glass panel subjected to blast loading is conducted using explicit dynamic analysis program LS-DYNA [28]. Based on the numerical result, the shape parameters ($\alpha$ and $\beta$) of the P-I curves are obtained using curve fitting.

### 4.1 Numerical model

Glass panels with two dimensions are chosen in accordance with the experiment tests reported by Ge et al. [12] and Zhang et al. [27], which are 1100mm×1100mm×8mm and 1500mm×1200mm×10mm respectively. In both tests, four sides of glass plies are fully clamped by steel window frames with certain embedded depths (100mm in Ge's test [12] and 50mm in Zhang's test [27]). The same boundary condition is simulated in numerical analysis. As shown in Figure 12, the glass ply is fixed into a steel frame with embedment on all sides in the FE model, and the thickness of steel plate is 5mm. The nodes on the surface of the steel frame are restrained in all directions to simulate a fix boundary condition. To simulate actual installation practice, a 2mm-thick cushion is inserted between the frame and the glass panel. The presence of a cushion layer also helps mitigate stress concentration, which could occur if the glass panel is just rigidly fixed to the steel frame in the FE model, leading to unrealistic premature failure of glass panel. It should be pointed out that such a treatment will tend to induce a difference between the boundary condition in the FE model and the assumed fixed boundary condition in the theoretical method. The possible influence of such a difference will be discussed in Section 4.2.

The blast loading is simulated by applying a simplified triangular decay uniform pressure on the outer surface of glass panel. As is discussed in section 3, the explosion distance should not be too close, or the assumption of uniform blast pressure cannot be justified. In Ge's test [12], the standoff distance is 5m, and the explosive was elevated at the same level as the panel centre (the panel size is 1100mm×1100mm). The resulting incident angle changes from a maximum value of 90° (at panel centre) to a minimum value of 83.72° (at panel corner) with a variation of 7%, and the corresponding propagation distance ranges from 5m to 5.05 with a variation of 1%, which are negligible. The variations of incident angle and propagation distance are also very small in Zhang's test [27]. It is therefore believed that the assumption of uniform blast pressure is justified in their tests.

The material properties employed in the FE analysis are listed in Table 3. Glass is a kind of brittle material with high elastic modulus. Therefore, the material type "ELASTIC" is employed for glass [16, 29-32], and the corresponding Poisson's ratio and mass density of the glass are taken as $v = 0.22$ and $\rho = 2560$ kg/m$^3$ respectively. Strength failure criterion is adopted to define the failure of glass. To simulate cracking, the erosion technique in LS-DYNA is employed in the FE analysis in conjunction with the strength criterion, which means the element will be deleted when its first principal stress exceeds the predefined failure stress. It should be noted that float glass and tempered glass were used respectively in the above two experiments. As is reported by Ge et al. [12], the failure strength for 8mm float glass is taken as 62.48 MPa based on flexure tests of the glass bar, and this value is adopted in the first numerical model. However, neither destructive tensile test nor bending test was conducted in Zhang's test [27] to quantity the failure stress of glass. The failure strength is therefore taken as 84Mpa for 10mm tempered glass in accordance with Chinese design standard JGJ102 [22] in the other model. For consistency, the same value is adopted in the proposed analytical model to generate the asymptotes of P-I curves. As the analysis focuses on the dynamic behaviour of the glass panel, the possible failure of the steel frame and cushion are not taken into consideration.

It should be noted that, in spite of its effectiveness, the above modelling method with erosion may not precisely simulate the details of the fragment shapes of glass, but it can well predict the dynamic response and failure modes of the whole glass panel [8, 29-31]. Therefore the modelling technique is considered as appropriate concerning the global dynamic response and the failures, which form the basis of proposing the analytical model of the P-I curves.

An 8-nodes element with one-point integration and hourglass control is adopted for all the materials in the FE model. The glass panel has been meshed into 3 layers along the thickness to simulate the bending effect, but neither the cushion nor the steel frame is further divided in thickness direction to save computing time. Based on a preliminary mesh convergence study, the element size of 5mm in both X and Y directions is determined. The results from the mesh convergence study indicate that further reduction of the mesh size would only introduce a negligible improvement of the numerical results but lead to a substantial increase in the computing time.

## 4.2 Numerical results and determination of α and β

The shape parameters ($\alpha$ and $\beta$) of the P-I curves are obtained based on the following process. Firstly, the post-crack behaviour of a glass panel is classified into 3 levels according to the damage characteristic and hazard level, as shown in Table 2. Then different combinations of pressure and impulse are applied in the numerical model to simulate the response of glass panel subjected to different blast loading. Thereafter, the behaviour of the glass panel corresponding to different combinations of pressure and impulse, such as damage state of glass panel and ejection speed of fragment, are extracted through numerical post-processing, and the boundaries between the predefined damage levels are identified. Based on these results, $\alpha$ and $\beta$ in Equation 1 can be obtained using curve fitting method. The fitted curves are shown with solid lines in Figure 13. It should be noted that $p_{cr}^k$ and $i_{cr}^k$ are calculated using the proposed analytical model, and the material parameters for glass are the same as those used in the numerical model. The calculated $p_{cr}^k$ and $i_{cr}^k$, together with the obtained shape parameters (*α* and *β*) are summarised in Table 4,

As can be seen in Table 4, *α* and *β* is around 2.5 and 1.5, respectively, and the variation of both parameters are within 5%. It is therefore believed that *α* and *β* are relatively insensitive to the change of damage level as well as panel size, thus in this study *α* and *β* are considered as constants by taking the average value of *α* and *β* in the above cases respectively, i.e. $\alpha = 2.48$ and $\beta = 1.48$. Therefore Equation 1 can then be expressed as

$$(p - p_{cr}^k)(i - i_{cr}^k) = 2.48\left(\frac{p_{cr}^k}{2} + \frac{i_{cr}^k}{2}\right)^{1.48} \tag{42}$$

Then the complete P-I curves of different damage levels for the glass panel can be generated according to Equation 42. As shown in Figure 13, P-I curves generated using a constant α and β (represented by dotted line) also show good agreement with numerical results, which demonstrates the effectiveness of adopting constant shape parameters for the P-I curves.

## 5. VERIFICATION OF THEORETICAL MODEL

### 5.1 Comparison of the Analytical Prediction and Test Result

For verification, the generated P-I curves are compared with experimental observations reported by Ge et al. [12] and Zhang et al. [27] (Figure 14). The test scenarios and corresponding ejection velocity of glass fragments are listed in Table 5.

As can be seen in Figure 14, the test results are basically located in the corresponding zones divided by theoretical P-I curves of different damage levels for both cases. In one of Ge's tests [12], a ejection velocity of 10.85m/s is measured when the glass panel is subjected to 1.6kg TNT charge exploded at a standoff distance of 5m. The tested peak overpressure and impulse are 139.76kPa and 174.92kPa·ms respectively. As is shown in Figure 14a, the corresponding coordinate point is very close to the generated P-I curve for a ejection velocity equals to 10m/s, which shows good accuracy. Further comparison is made for a different size of glazing according to ref. [27]. It should be noted that two panels were tested for one blast in Zhang's test, and totally 6 available testing results were obtained from 4 loading cases. As can be observed in Figure 14b, one of the loading conditions ($p$=130.12kPa and $i$=377.73kPa·ms) is situated very close to the P-I curve corresponding to ejection velocity=10m/s, and the measured velocity is 11.6m/s and 13.7m/s for two specimens respectively. Comparison indicates that the predicted ejection velocity of glass fragment is a little underestimated. This difference can be partly attributed to the material properties of glass may be different from the tempered glass used in the tests. Meantime, as field test is strongly affected by on-site conditions, the obtained experimental data exhibits some variation. For example, in another testing case, a higher ejection velocity ($v$=16.4m/s) is measured when the panel is subjected to a smaller blast loading ($p$=84.69kPa and $i$=296.78kPa·ms), which may result in the derivation between numerical prediction and test results. In general, the P-I curves generated in current study fit well with test results.

The agreement between FE result and experimental result in dynamic region indicates that the FE model can well predict the dynamic response of glass panels subjected to blast loading. Besides, the correctness of the shape parameters is well justified. However, due to the limitation of experiment data, only the dynamic region of P-I curve has been verified by experimental data. A validation against further numerical simulation is carried out for both impulse region and quasi-static region in the following section.

## 5.2 Comparison of the Analytical Prediction and Numerical Result

In order to validate the theoretical results of the impulse asymptotes and overpressure asymptotes of P-I curve of different damage levels, additional FE analysis is conducted in both the impulse and quasi-static regions, using the same FE model as introduced in section 4.1. A series of numerical tests are carried out with different blast loadings, and the corresponding combinations of overpressure and impulse are set around the asymptotes calculated from the theoretical method. The comparisons are shown in Figure 15 and Table 6.

As can be seen, the results from the numerical simulation and theoretical method are generally in good agreement. The data points situated in the impulse region and in the quasi-static region for different damage levels match well with the respective impulse and overpressure asymptotes predicted by theoretical method. The discrepancies of the results are within about 15%, except for the impulse asymptote of damage level I $i_{cr}^{I}$. For the 1100mm×1100mm×8mm panel, the obtained $i_{cr}^{I}$ is 43kPa·ms in numerical simulation, while that is 36.05kPa·ms by theoretical method with a maximum discrepancy of -16.17%. For the panel with dimension of 1500mm×1200mm×10mm, the discrepancy is -16.26%. The discrepancy may be partly attributed to the idealised fixed boundary conditions in the analytical model, but more attributed to the inconsistent movement of glass panel during dynamic response. In order to improve the accuracy of the calculated $i_{cr}^{I}$, an adjust coefficient is proposed later to minimise errors due to the inconsistent movement, which will be further discussed in the section 6.1.

On the whole, the proposed simplified analytical model provides satisfactory prediction of the impulse asymptote and overpressure asymptote of different damage levels, and the constant shape parameters $\alpha$ and $\beta$ obtained from numerical analysis also show good agreement with experimental results.

# 6. DISCUSSIONS

## 6.1 Influence of Inconsistent Movement

As is discussed in section 5.2, the $i_{cr}^{I}$ calculated by the theoretical model shows considerable error with the numerical results for damage level I. The main reason should be attributed to the inconsistent movement of the glass panel during the dynamic response. The inconsistent movement refers to the situation where the movement of the glass panel at different locations is not precisely synchronized to follow a given mode of deflection, as can be expected in an actual situation. For example, when the velocity at the panel centre becomes zero at a peak response, the velocity at the panel corner may be non-zero, thus resulting in a certain amount of kinetic energy. The inconsistent movement cannot be included if only one deflection mode is considered in calculation, as in that case the motion of whole panel is dominated by panel centre, and the velocity of each point on the panel can be 0m/s simultaneously. However, high modes of motion can be excited when the glass panel is subjected to blast loading, and the existence of inconsistent movement will result in derivation.

Figure 16 shows the energy time history for the 1100mm×1100mm×8mm panel under impulsive loading, and the corresponding overpressure and impulse are 2000kPa and 60kPa·ms respectively corresponding to damage level I, the onset of glass crack. As can be seen, the kinetic energy $E_k$ increases rapidly due to the initial loading and then gradually transform into internal strain energy.

At t=3.4ms, the kinetic energy decreases to a minimum value of 3.44J while the internal energy rises to a peak value of 17.79J. At the same time, the panel reaches its maximum deflection and glass cracks. It shows that at the failure moment, the initial kinetic energy $E_{k0}$ cannot completely transform into strain energy $U_i$, and a certain amount of kinetic energy resulting from the inconsistent movement remains. The existence of $E_{kr}$ will lead to an increase of the imparted energy to cause glass fracture. In other words, the bearing capacity in theoretical model tends to be underestimated as $E_{kr}$ is ignored for damage level I, resulting in a conservative estimation.

It can also be noted that the influence of inconsistent movement would cause relatively larger error for the impulse asymptote of damage level I (glass crack limit) than that of damage level II (eject with certain velocity). For the later damage levels, the proportion of the kinetic energy related to inconsistent movement of panel becomes negligible in comparison with the totla kinetic energy related to the flying of glass fragments. That also explains why the discrepancy between theoretical results and numerical results decreases with the increase of ejection velocity (Table 6). In order to reduce the error for theoretical result of the impulse asymptote of damage level I, an adjust coefficient $\xi$ is proposed.

$$i_c^1 = \xi \times i_{cr}^1 \tag{43}$$

Based on the above discussion, the $i_{cr}^I$ is re-given by Equation 44 to take the influence of residual kinetic energy into consideration.

$$i_{cr}^I = \frac{1}{ab}\sqrt{2M_e(U_i + E_{kr})} \tag{44}$$

where $U_i$ and $E_{kr}$ are the internal energy and the residual kinetic energy of glass panel at failure moment respectively.

Through the comparison between Equation 17 and 44, the adjust coefficient $\xi$ can be written as

$$\xi = \sqrt{\frac{U_i + E_{kr}}{U_i}} \tag{45}$$

Here, another index $\lambda = \frac{E_{kr}}{U_i + E_{kr}}$ is introduced to represent the ratio of residual kinetic energy to total energy at failure moment, which can reflect the influence of inconsistent movement of glass panel for damage level I. According to Equation 45, the relationship between $\xi$ and $\lambda$ can then be obtained as

$$\xi = \sqrt{\frac{1}{1-\lambda}} \tag{46}$$

To determine the value of $\lambda$, a numerical parametric analysis in terms of panel size and glass thickness is conducted, and the corresponding parameters are shown in Table 7. The numerical model is the same as introduced in section 4.1 and the failure stress of different glass panels are uniformly taken as 60MPa. The blast loading applied in each case corresponds to the glass crack threshold and is pre-determined numerically. The values of internal energy, kinetic energy and total energy at glass failure moment are extracted for each case, and the corresponding $\lambda$ can be obtained. It is found that the ratio $\lambda$ is linearly correlated to the first vibration period of glass panel $T_s$, as shown in Figure 17. Thus the relationship between $\lambda$ and $T_s$ is given by

$$\lambda = 0.0025T_s + 0.18 \tag{47}$$

It should be pointed out that the modification coefficient $\xi$ is suitable for glass panel with the natural period within the range of 5ms to 45ms, which basically covers the commonly used glass windows. The main function of $\xi$ is to modify the impulse asymptote of damage level I to consider the inconsistent movement. As listed in Table 8, after adjustment for theoretical results, the corresponding errors reduce from -16.17% to -5.26% and from -16.26% to -4.53% respectively, indicating the accuracy of theoretical results is improved.

## 6.2 Influence of the Shearing Region Width Ds

It is worth noting that the assumed shearing region width $D_s$ has a significant influence on the value of impulse asymptote of damage level II. The reason is that for punching failure mode, the internal strain energy mainly stores in the shearing region near boundaries, thus the width of the shearing region can directly affect the amount of stored strain energy in the glass panel before fracture and then the corresponding theoretical result of $i_{cr}^{k}$. Detailed numerical simulation for the panel of 1100mm×1100mm×8mm shows that with the increase of ejection velocity the width of the shearing region decreases (Figure 18), and punching failure mode becomes more obvious. When the ejection velocity is relatively small, the failure mode is a combination of bending failure and punching failure, which is different from the assumed punching failure mode and may consequently cause a larger error in the results using the proposed analytical method.

It may be argued that a clear punching failure occurs only when the kinetic energy $E_{kr}$ is large enough, wherein the validity of the theoretical method can be guaranteed. As can be seen in Figure 19, with the increase of imparted impulse, the proportion of the residual kinetic energy tends to increase and the punching failure mode of the panel becomes increasingly dominant, for which a critical residual kinetic energy ratio $\lambda_c$=0.8 is suggested as the low limit to ensure the occurrence of punching failure. Then the corresponding critical velocity $v_{rc}$ is given by Equation 48.

$$v_{rc} = \sqrt{\frac{2E_i}{M_e(1-\lambda_c)}} \tag{48}$$

Accordingly, the critical ejection velocity for the 1100mm×1100mm×8mm glass panel can be obtained, which is about 10m/s. Here a critical damage level is defined as the glass fragments eject at the critical velocity ($v_{rc}$), and different shearing region widths are adopted in the theoretical calculation. The obtained results are summarized in Table 9. As can be observed, the theoretical impulse asymptote of the critical damage level is in good agreement with the FEA result ($i_{cr}$=140kPa·ms) when the width of the shearing region equals 5$h$, where $h$ is the thickness of glass panel. Therefore, 5$h$ is a recommended value for the shearing region width for critical damage level under impulsive loading ($D_{sc}$) in the present study. Further study is needed to provide a more rigorous prediction of $D_{sc}$.

As is discussed above, punching failure mode becomes increasingly dominant when ejection velocity increases, resulting in the decrease of the shearing region width. In order to determine the width of the shearing region $D_s$ for an arbitrary velocity $v_r$ that exceeds the critical velocity $v_{rc}$, an empirical formula is developed based on numerical parametric study, as shown in Equation 49. The width of the shear region shows an exponential decay with the increase of the ejection velocity, and it eventually approaches a simple impulse-momentum transfer ($D_s$=0).

$$D_s = D_{sc} e^{-(v_r - v_{rc})}, v_r \geq v_{rc} \tag{49}$$

## 7. CONCLUSIONS

In this paper, a theoretical method is proposed to build the P-I curves for framed monolithic glass panel for different damage levels, in particular a) the onset of glass crack and b) the fragments eject with a specified velocity. Based on the observed failure modes from finite element simulations, the pressure asymptote and the impulse asymptote are derived analytically, whereas the dynamic segment of the curve is established using an empirical approach based on numerical simulation results.

The method is verified with published experiment results and against additional numerical tests. The effects of inconsistent movement at the bending failure limit and the possible variation of the shearing region size are discussed. Based on numerical parametric analyses, empirical formulae for the modification coefficient $\xi$ and shearing region width $D_s$ are proposed. It is shown that the modified theoretical model improves the prediction results.

The proposed theoretical model can be used to establish the P–I diagrams for framed monolithic glass windows with variable dimension, which provides a practical approach for estimation of splashing distance and thereafter hazard assessment for an existing design, as well as for a new blast resistant design of glazing for a required hazard level.

## ACKNOWLEDGEMENTS

The authors gratefully acknowledge the financial support by the National Natural Science Foundation of China under the grant No.51278365 and the State Key Laboratory for Disaster Reduction in Civil Engineering, Tongji University under the grant No. SLDRCE 14-B-13.

## REFERENCES

1]. Norville, H.S., Harvill, N.C., Edward, J., Shariat, S. and Mallonee, S., *Glass-Related Injuries in Oklahoma City Bombing*. Journal of Performance of Constructed Facilities, 1999. **13**(2): p. 50-56.
2]. GSA-TS01-2003, *Standard Test Method for Glazing and Window Systems Subject to Dynamic Overpressure Loadings*. 2003.
3]. ASTM-F2248-12, *Standard Practice for Specifying an Equivalent 3-Second Duration Design Loading for Blast Resistant Glazing Fabricated with Laminated Glass*. 2012.
4]. ASTM-E1300-12a, *Standard Practice for Determining Load Resistance of Glass in Buildings*. 2012.
5]. Meyers, G.E., *Design Criteria and Preliminary Acceptance Test Specifications for Blast Resistant Windows.* Design Criteria & Preliminary Acceptance Test Specifications for Blast Resistant Windows, 1984.

6]. Pritchard, D.K., *Breakage of glass windows by explosions.* Journal of Occupational Accidents, 1981. **3**(2): p. 69-85.

7]. Cormie, D., Mays, G.C. and Smith, P.D., *Blast effects on buildings, second ed.* 2009, England Thomas Telford Publications.

8]. Hooper, P.A., Sukhram, R.A.M., Blackman, B.R.K. and Dear, J.P., *On the blast resistance of laminated glass.* International Journal of Solids & Structures, 2012. **49**(6): p. 899-918.

9]. Zhang, X.H., Hao, H. and Ma, G.W., *Parametric study of laminated glass window response to blast loads.* Engineering Structures, 2013. **56**(6): p. 1707-1717.

10]. Meyers, G.E., Baldwin, P.E.D. and Mlakar, P.E.P., *State of the art of blast resistant windows.* Occupational Health Nursing, 1978. **23**(23): p. 72-91.

11]. Larcher, M., Solomos, G., Casadei, F. and Gebbeken, N., *Experimental and Numerical Investigations of Laminated Glass Subjected to Blast Loading.* International Journal of Impact Engineering, 2012. **39**(1): p. 42-50.

12]. Ge, J., Li, G.Q. and Chen, S.W., *Theoretical and experimental investigation on fragment behavior of architectural glass panel under blast loading.* Engineering Failure Analysis, 2012. **26**(12): p. 293–303.

13]. Zhang, X., Hao, H. and Wang, Z., *Experimental Investigation on Monolithic Tempered Glass Window Responses to Blast Loads.* International Journal of Protective Structures, 2015. **6**(2): p. 287-309.

14]. Johns, R.V. and Clubley, S.K., *Post-fracture response of blast-loaded monolithic glass.* Structures & Buildings, 2015. **168**(7): p. 1-10.

15]. Spiller, K., Packer, J.A., Seica, M.V. and Yankelevsky, D.Z., *Prediction of annealed glass window response to blast loading.* International Journal of Impact Engineering, 2016. **88**: p. 189-200.

16]. Pelfrene, J., Kuntsche, J., Dam, S.V., Paepegem, W.V. and Schneider, J., *Critical assessment of the post-breakage performance of blast loaded laminated glazing: experiments and simulations.* International Journal of Impact Engineering, 2016. **88**.

17]. Shi, Y., Hao, H. and Li, Z.X., *Numerical derivation of pressure–impulse diagrams for prediction of RC column damage to blast loads.* International Journal of Impact Engineering, 2008. **35**(11): p. 1213-1227.

18]. Krauthammer, T. and Altenberg, A., *Negative phase blast effects on glass panels.* International Journal of Impact Engineering, 2000. **24**(1): p. 1-17.

19]. Wei, J. and Dharani, L.R., *Response of laminated architectural glazing subjected to blast loading.* International Journal of Impact Engineering, 2006. **32**(12): p. 2032-2047.

20]. Timoshenko, S.P., *Theory of plates and shells.* Studies in Mathematics & Its Applications Elsevier Amsterdam, 1940. **6**(3760): p. 606.

21]. Biggs, J.M., *Introduction to structural dynamics*. 1964.

22]. JGJ-102, *Technical code for glass curtain wall engineering*, in Ministry of Housing and Urban-Rural Development of the People's Republic of China. 2003.

23]. Anderson, T.L., *Fracture mechanics : fundamentals and applications*. 2005: Taylor & Francis.

24]. Wiederhorn, S.M., *Fracture Surface Energy of Glass.* Journal of the American Ceramic Society, 1969. **52**(2): p. 99–105.

25]. Griffith, A.A., *The Phenomena of Rupture and Flow in Solids.* Philosophical Transactions of the Royal Society of London, 1921. **221**: p. 163-198.

26]. Van Doormaal, A., Weerheijm, J. and Rhijnsburger, M. *Hazard of Glazing Due to Blast Loading*. In Hazard of Glazing Due to Blast Loading Tno Repository. 2007.

27]. Zhang, X., Hao, H. and Wang, Z., *Experimental investigation of monolithic tempered glass fragment characteristics subjected to blast loads.* Engineering Structures, 2014. **75**: p. 259–275.

28]. LS-DYNA Keyword user's manual, *Livermore Software Technology Corporation*. 2007.

29]. Belis, J., Depauw, J., Callewaert, D., Delincé, D. and Impe, R.V., *Failure mechanisms and residual capacity of annealed glass/SGP laminated beams at room temperature.* Engineering Failure Analysis, 2009. **16**(6): p. 1866-1875.

30]. Chen, S.W., Zhu, C.G., Li, G.Q. and Ge, J., *Blast test and finite element analysis of point-supported glass curtain wall.* Journal of Building Structures, 2012. **33**(12): p. 99-105.

31]. Wei, Y. and Chen, S.W., *Introduction of the simplified analysis and design for blast-resistance of glazing curtain wall.* Doors & Windows, 2009.

32]. Pelfrene, J., Dam, S.V., Paepegem, W.V. and Degrieck, J. *Numerical simulation of elastic, fracture and post-failure response of monolithic and laminated glass under impact loading*. In Cost Action TU0905 Mid-Term Conference on Structural Glass. 2013.

Table 1: Glass-Related Injuries by Buildings in Proximity to Ground Zero [1]

| Building number | Building name | Total bomb-related injuries | Glass-related injuries |
|---|---|---|---|
| 1 | Alfred P. Murrah Federal Building | N/A | N/A |
| 2 | Durham Post Office | 7 | 3 |
| 3 | Water Resources Board | 39 | 23 |
| 4 | Athenian Restaurant | 4 | 2 |
| 5 | YMCA | 81 | 33 |
| … | … | … | … |

Table 2: Classification of damage levels

| Damage level | Features of performance under blast loading |
|---|---|
| I | Glass crack limit |
| II | The ejection velocity $v_r$ = 10m/s |
| III | The ejection velocity $v_r$ = 20m/s |

Table 3: Material properties adopted in FEA

| Material | Material model | Material No. in Ls-dyna | Density (Kg/m$^3$) | Elasticity module (N/m$^2$) | Poisson's ratio | Failure criterion |
|---|---|---|---|---|---|---|
| Float glass | Elastic | MAT_001 | 2.56e3 | 7.2e10 | 0.22 | $\sigma_1$=62.48MPa or 84MPa * |
| Steel | Plastic_Kinematic | MAT_003 | 7.86e3 | 2.1e11 | 0.288 | —— |
| Silicon cushion | Elastic | MAT_001 | 1e3 | 1e8 | 0.45 | —— |

* The failure criterions are adopted for two different cases respectively, 62.48MPa for Ge's test [12] and 84MPa for simulating Zhang's test [27].

Table 4: Shape parameters of P-I curve

| Dimension (mm×mm) | Glass thickness (mm) | Damage level | Theoretical result | | Shape parameters | |
|---|---|---|---|---|---|---|
| | | | $P_{cr}$ | $i_{cr}$ | α | β |
| 1100×1100 | 8 | I (Glass crack) | 12.60 | 36.05 | 2.41 | 1.53 |
| | | II ($v_r$ = 10m/s) | 69.98 | 149.16 | 2.49 | 1.43 |
| | | III ($v_r$ = 20m/s) | 242.04 | 199.90 | 2.53 | 1.50 |
| 1500×1200 | 10 | I (Glass crack) | 23.79 | 52.34 | 2.55 | 1.51 |
| | | II ($v_r$ = 10m/s) | 103.8 | 194.1 | 2.42 | 1.45 |
| | | III ($v_r$ = 20m/s) | 323.83 | 255.64 | 2.50 | 1.47 |
| Average value | | | | | 2.48 | 1.48 |

Table 5: Experimental results by Ge et al. [12] and Zhang et al. [27]

| Dimension (mm×mm) | Thickness (mm) | TNT Charge (kg) | Standoff distance (m) | Impulse (kPa·ms) | Overpressure (kPa) | Measured ejection velocity (m/s) |
|---|---|---|---|---|---|---|
| 1100×1100 [12] | 8 | 0.6 | 5 | 87.77 | 72.88 | 3.49 |
| | | 0.8 | 5 | 107.35 | 87.08 | 3.83 |
| | | 1.2 | 5 | 142.79 | 113.9 | 6.62 |
| | | 1.6 | 5 | 174.92 | 139.76 | 10.85 |
| 1500×1200 [27] | 10 | 5 | 6 | 363.86 | 219.99 | 16.4 |
| | | 5 | 8 | 377.73 | 130.12 | 11.6 |
| | | 5 | 8 | 377.73 | 130.12 | 13.7 |
| | | 10 | 12 | 296.78 | 84.69 | 16.4 |
| | | 10 | 9 | 459.35 | 141.47 | 25.4 |
| | | 10 | 9 | 459.35 | 141.47 | 18.5 |

Table 6: Comparison between the asymptotes obtained from theoretical results and FEA results

| Dimension (mm×mm) | Glass thickness (mm) | Damage level | FEA result | | Theoretical result | | | |
|---|---|---|---|---|---|---|---|---|
| | | | $p_{cr}$ (kPa) | $i_{cr}$ (kPa·ms) | $p_{cr}$ (kPa) | error | $i_{cr}$ (kPa·ms) | error |
| 1100×1100 | 8 | I (Glass crack) | 13 | 43 | 12.60 | -3.08% | 36.05 | -16.17% |
| | | II ($v_r$ = 10m/s) | 80 | 140 | 69.98 | -12.53% | 149.16 | 6.54% |
| | | III ($v_r$ = 20m/s) | 250 | 220 | 242.04 | -3.18% | 199.90 | -9.13% |
| 1500×1200 | 10 | I (Glass crack) | 22.5 | 62.5 | 23.79 | 5.73% | 52.34 | -16.26% |
| | | II ($v_r$ = 10m/s) | 110 | 210 | 103.8 | -5.64% | 194.10 | -7.57% |
| | | III ($v_r$ = 20m/s) | 310 | 270 | 323.83 | 4.46% | 255.64 | -5.32% |

Note：The corresponding errors between simplified theoretical model and FEA result equal to $\frac{P_{Theoretical}-P_{FEA}}{P_{FEA}}$ or $\frac{i_{Theoretical}-i_{FEA}}{i_{FEA}}$.

Table 7: Summary of numerical parametric analysis results

| Case No. | $a$ (m) | $b$ (m) | thickness (mm) | $T_s$ (ms) | $i_{FEA}$ (kPa·ms) | Kinetic Energy (J) | Internal Energy (J) | Total Energy (J) | $\lambda$ |
|---|---|---|---|---|---|---|---|---|---|
| test 1 | 1.75 | 1.75 | 6 | 42.71 | 35 | 5.35 | 15.40 | 20.15 | 0.27 |
| test 2 | 1.50 | 1.50 | 6 | 30.67 | 38 | 4.75 | 14.11 | 18.33 | 0.26 |
| test 3 | 1.00 | 1.00 | 6 | 14.23 | 40 | 1.60 | 6.51 | 7.94 | 0.20 |
| test 4 | 0.50 | 0.50 | 6 | 3.85 | 40 | 0.72 | 3.23 | 3.87 | 0.19 |
| test 5 | 1.88 | 1.20 | 6 | 26.58 | 29 | 3.61 | 11.15 | 14.35 | 0.25 |
| test 6 | 2.25 | 1.00 | 6 | 20.31 | 23 | 2.74 | 10.06 | 12.81 | 0.21 |
| test 7 | 2.50 | 0.90 | 6 | 16.89 | 23 | 2.24 | 9.41 | 11.65 | 0.19 |
| test 8 | 1.50 | 1.50 | 8 | 24.74 | 47 | 4.24 | 13.58 | 17.82 | 0.24 |
| test 9 | 1.50 | 1.50 | 10 | 20.77 | 53 | 5.79 | 18.24 | 24.03 | 0.24 |
| test 10 | 1.50 | 1.50 | 12 | 17.94 | 68 | 6.93 | 26.44 | 33.37 | 0.21 |

Table 8: Theoretical result after modification for inconsistent movement

| Dimension (mm×mm) | Glass thickness (mm) | $Ts$ (ms) | $i_{FEA}$ (kPa·ms) | Theoretical $i_{cr}$ for damage level I (kPa·ms) | | Adjust coefficient $\xi$ |
|---|---|---|---|---|---|---|
| | | | | Before modification | After modification | |
| 1100×1100 | 8 | 16.26 | 43 | 36.05 (-16.17%) | 40.73 (-5.26%) | 1.13 |
| 1500×1200 | 10 | 18.65 | 62.5 | 52.34 (-16.26%) | 59.66 (-4.53%) | 1.14 |

Note：Values in parentheses are corresponding error between simplified theoretical model and FEA result, which equals to $\dfrac{i_{Theoretical} - i_{FEA}}{i_{FEA}}$.

Table 9: Theoretical results of impulse asymptote for different $D_s$ for critical damage level

| $D_s/h$ | 2 | 3 | 4 | 5 | 6 |
|---|---|---|---|---|---|
| $i_{cr}$ ($v_r$ =10m/s) | 94.84 | 106.53 | 124.85 | 149.16 | 178.42 |

Figure 1: Performance classification for window system response in GSA/ISC[2].

Figure 2. Simplified analytical model

Figure 3. Simplified blast wave

Figure 4. ISO damage curves under different damage levels

Figure 5. Failure modes of glass panels subjected to different impulsive loading

Figure 6. Deflection profiles at the window centre line under impulsive loading (Damage level I), based on FE simulation

Figure 7. Comparison of deflection profiles between FEA result and theoretical hypothesis for impulsive region (Damage level I)

Figure 8. Displacement and stress distribution of glass panel under impulsive loading (Damage level II), based on FE simulation

Figure 9. Deflection profile near the window border under impulsive loading (Damage level II), based on FE simulation

Figure 10. Simplified beam model; beam length = $D_s$

Figure 11. A typical fragment with sides of $\Delta a$ in a glass ply

Figure 12. FE model

Figure 13. Comparison between the generated P-I curves and FEA results in dynamic region

Figure 14: Comparison between the generated P-I curves and experimental results

Figure 15. Comparison between the generated P-I curves and FEA results in impulsive and quasi-static regions

Figure 16. Time history of kinetic energy and internal energy for damage level I in impulsive asymptote, based on FE analysis

Figure 17. Incomplete conversion coefficient of kinetic energy

Figure 18. Deflection profiles at failure time for different ejection velocity under impulsive loading, based on FE analysis

Figure 19. Relationship between energy ratio and imparted impulse

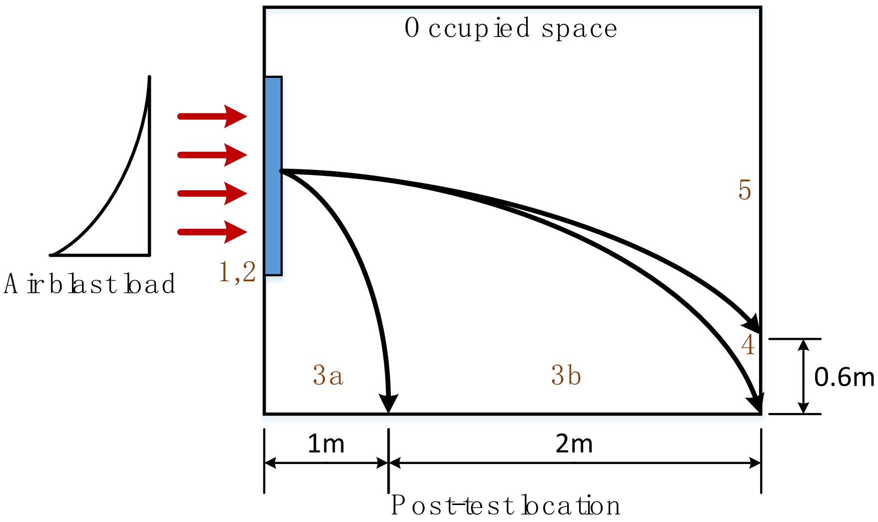


Figure 1: Performance classification for window system response in GSA/ISC[2].

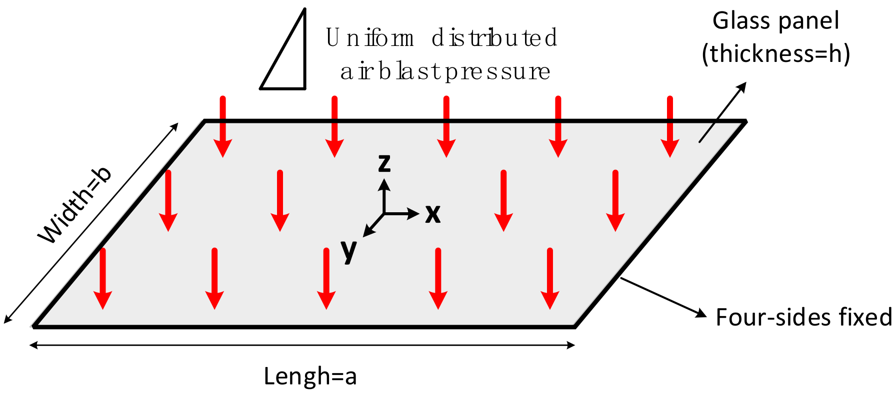


Figure 2. Simplified analytical model

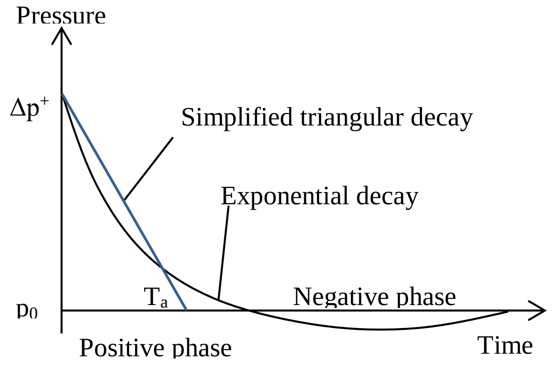


Figure 3. Simplified blast wave

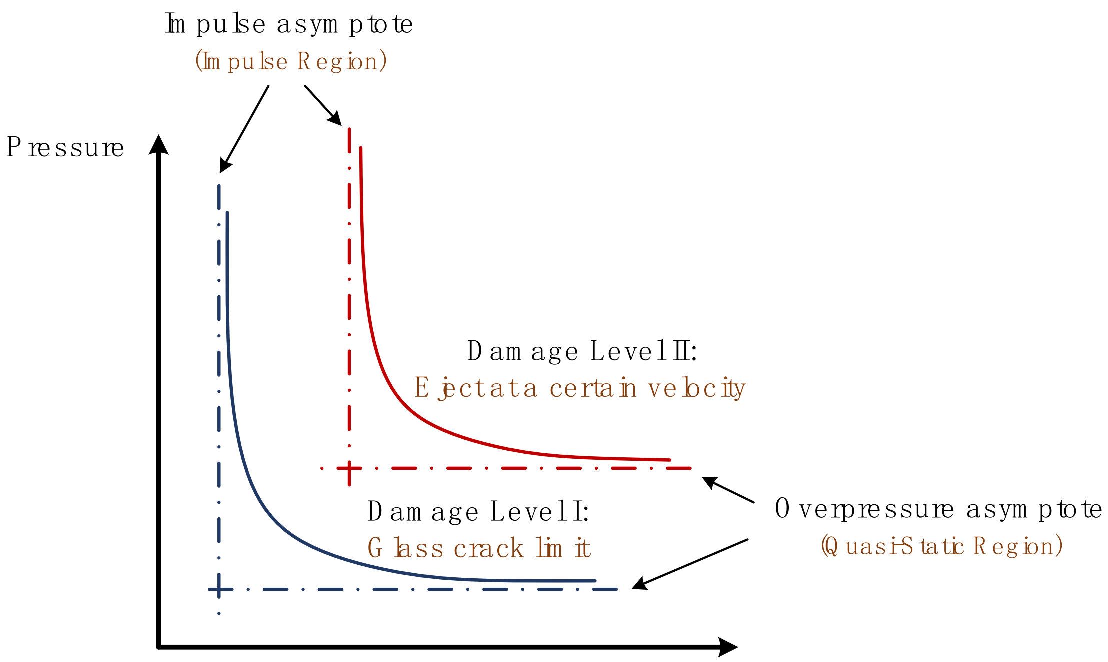


Figure 4. ISO damage curves under different damage levels

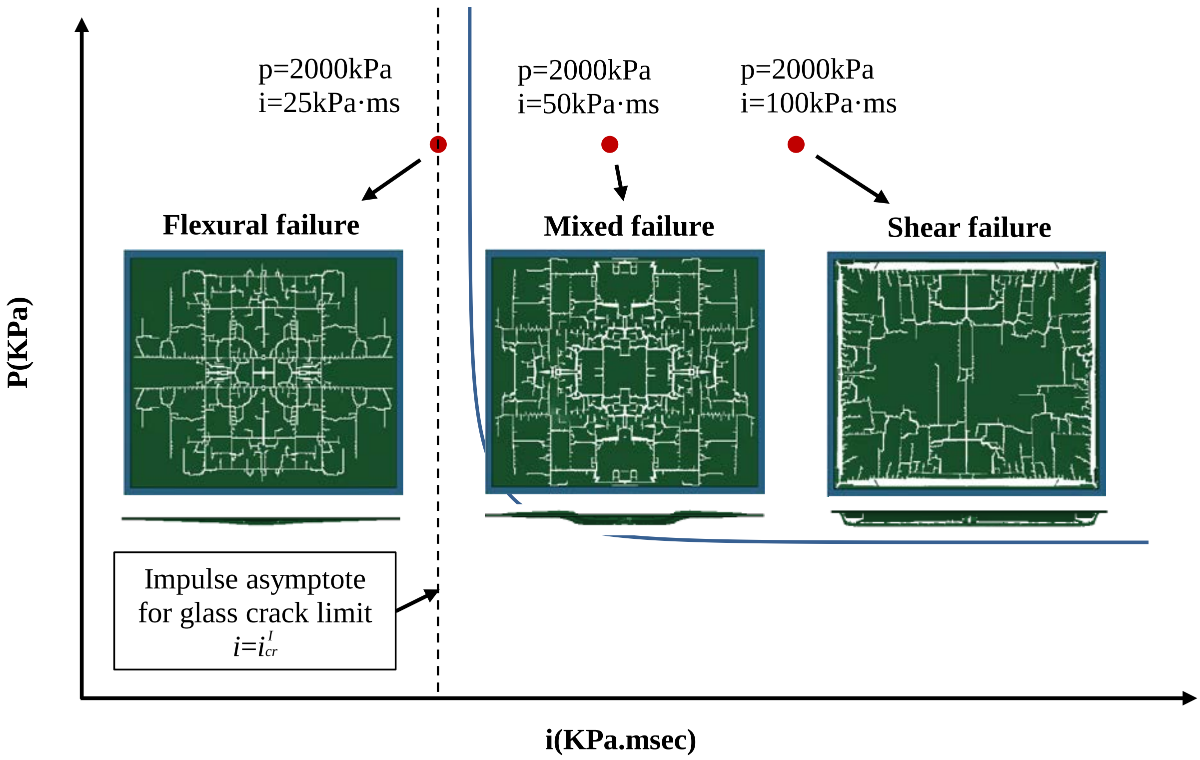


Figure 5. Failure modes of glass panels subjected to different impulsive loading

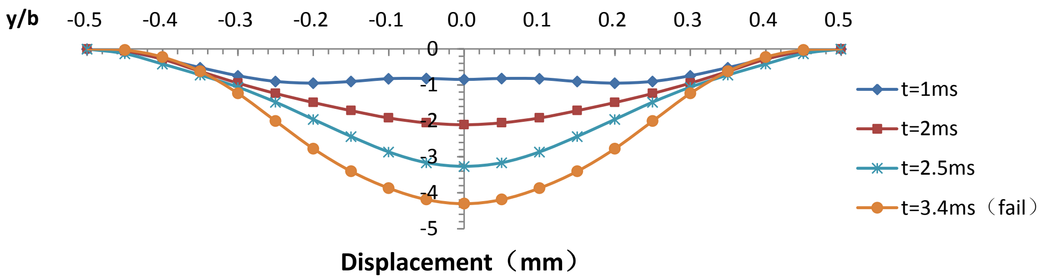


Figure 6. Deflection profiles at the window centre line under impulsive loading (Damage level I), based on FE simulation

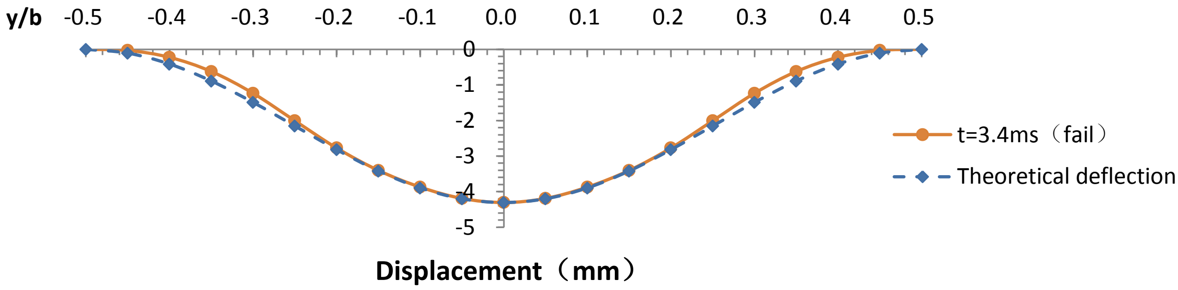


Figure 7. Comparison of deflection profiles between FEA result and theoretical hypothesis for impulsive region (Damage level I)

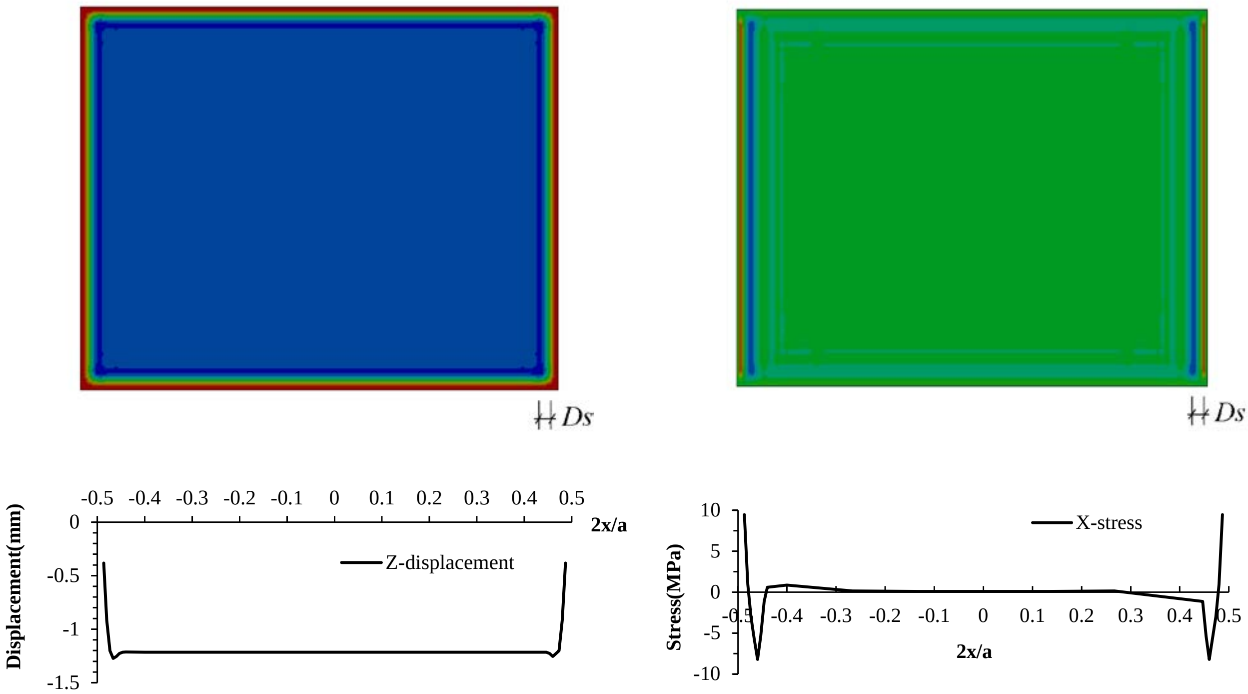


a. z-displacement profile

b. x-stress profile

Figure 8. Displacement and stress distribution of glass panel under impulsive loading (Damage level II), based on FE simulation

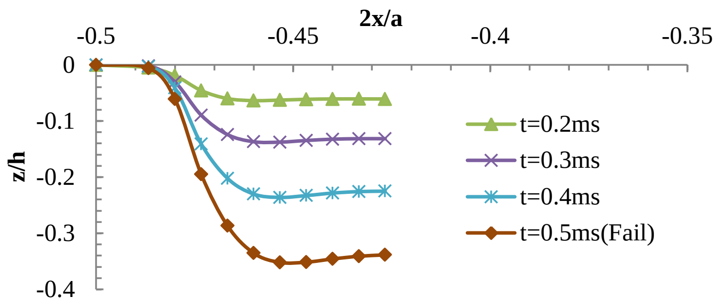


Figure 9. Deflection profile near the window border under impulsive loading (Damage level II), based on FE simulation

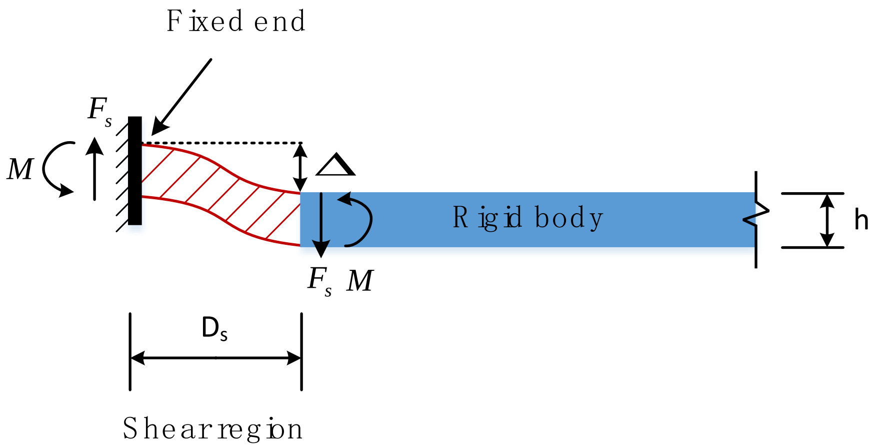


Figure 10. Simplified beam model; beam length = $D_s$

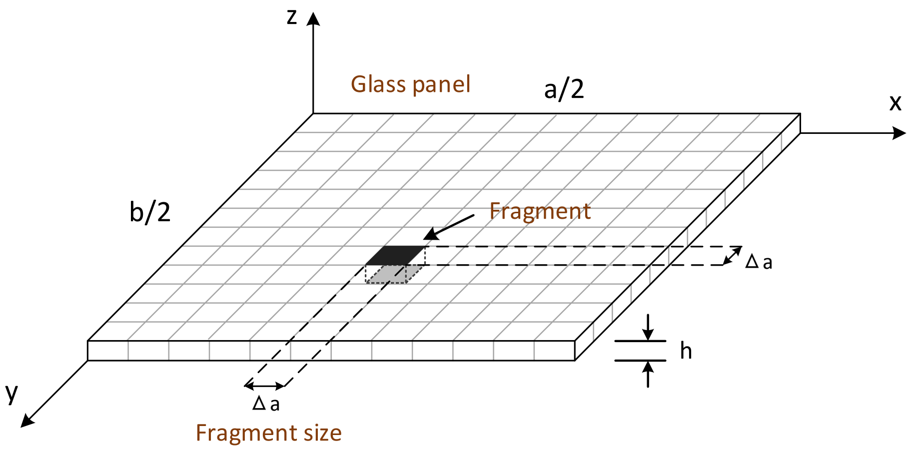

Figure 11. A typical fragment with sides of ∆a in a glass ply

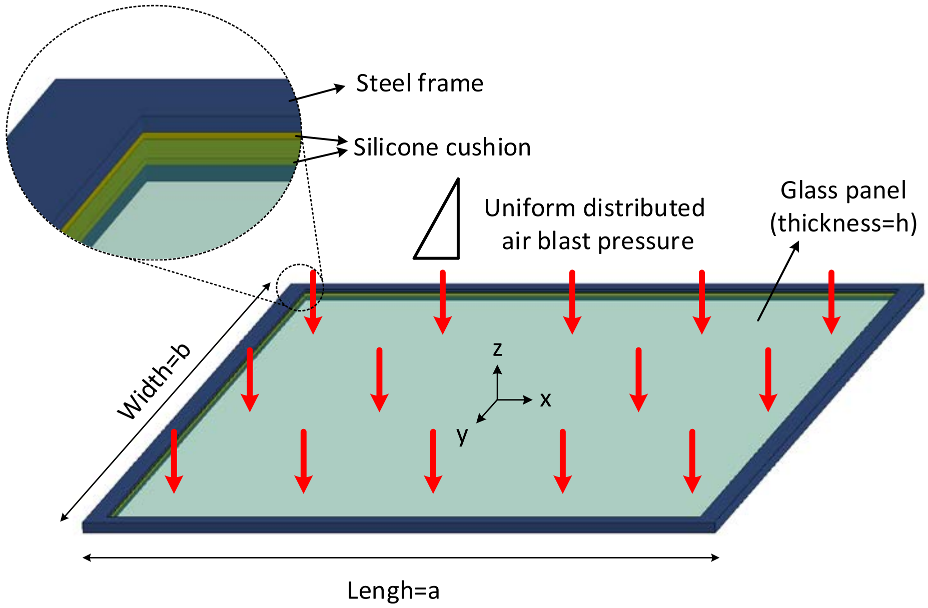


Figure 12. FE model

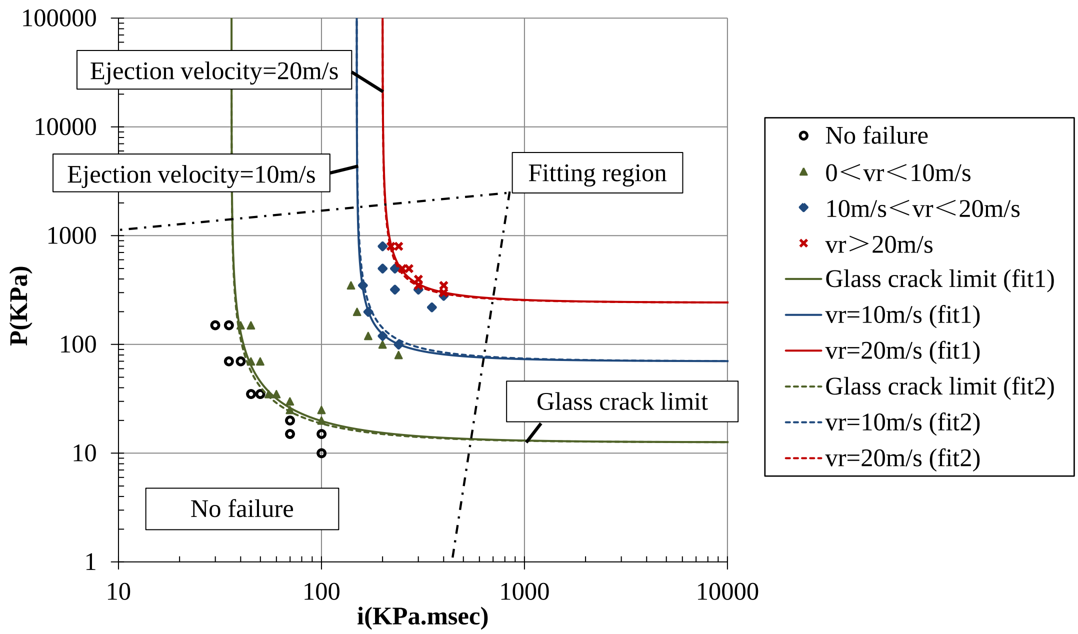


a. 1100mm×1100mm×8mm glass panel.

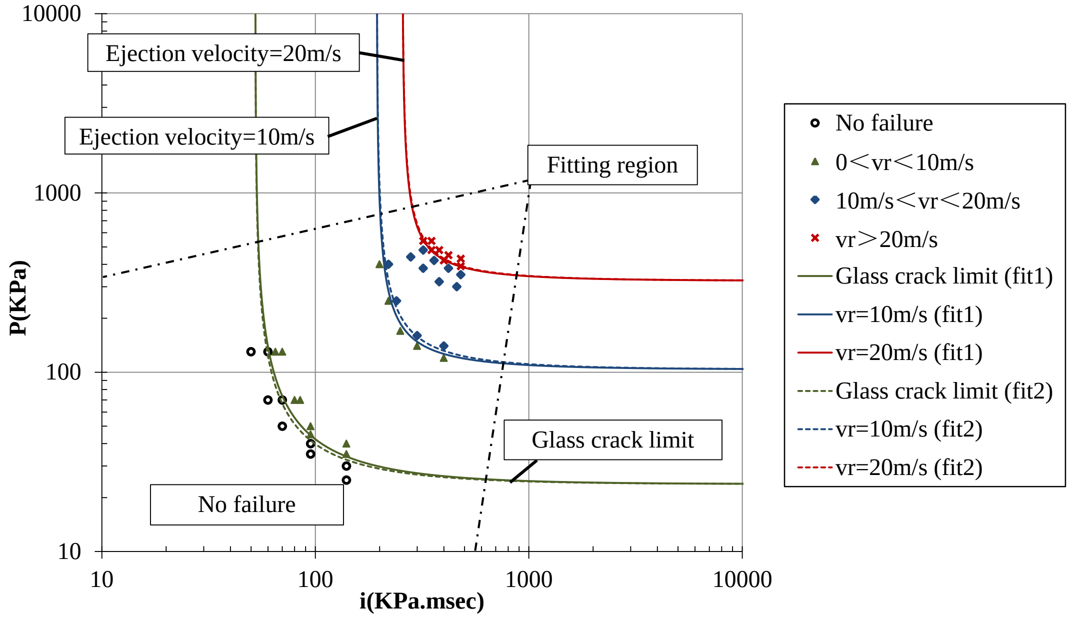


b. 1500mm×1200mm×10mm glass panel.

Figure 13. Comparison between the generated P-I curves and FEA results in dynamic region

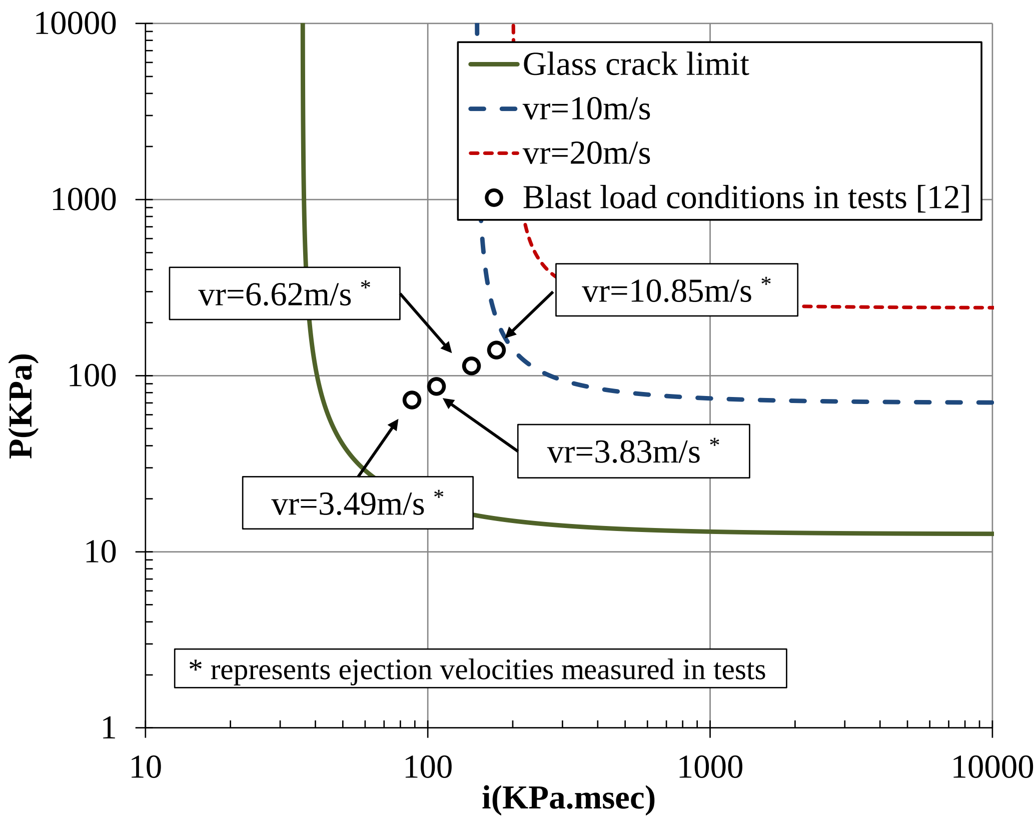


a. 1100mm×1100mm×8mm glass panel.

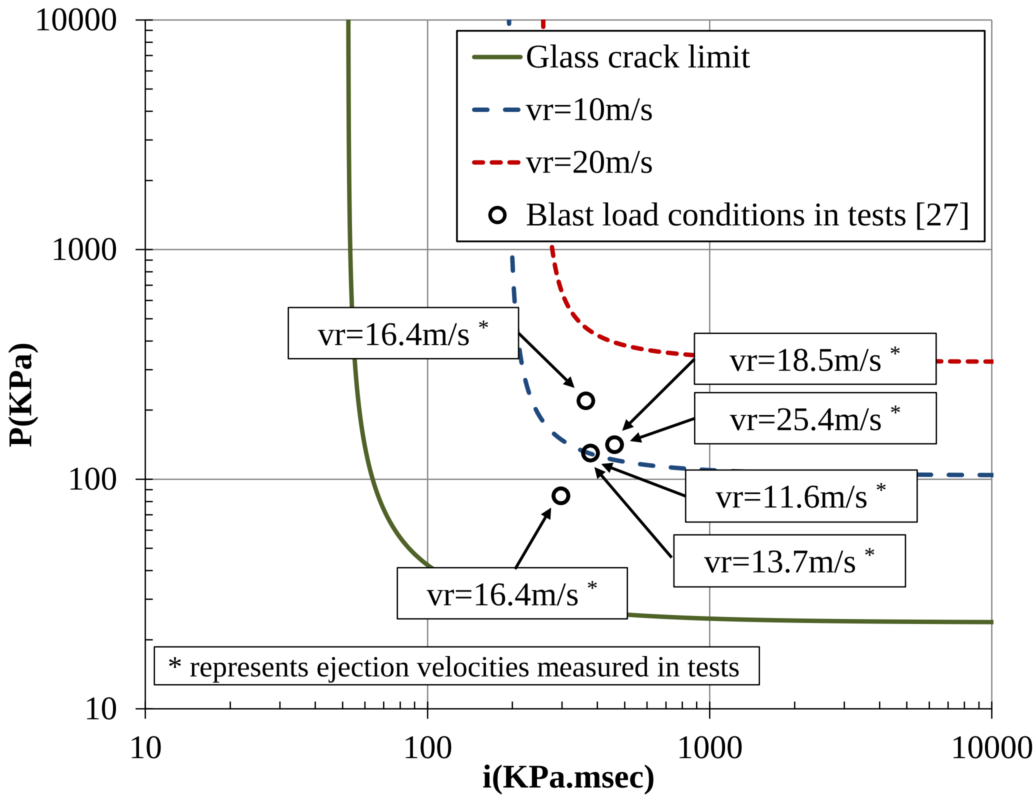


b. 1500mm×1200mm×10mm glass panel.

Figure 14. Comparison between the generated P-I curves and experimental results

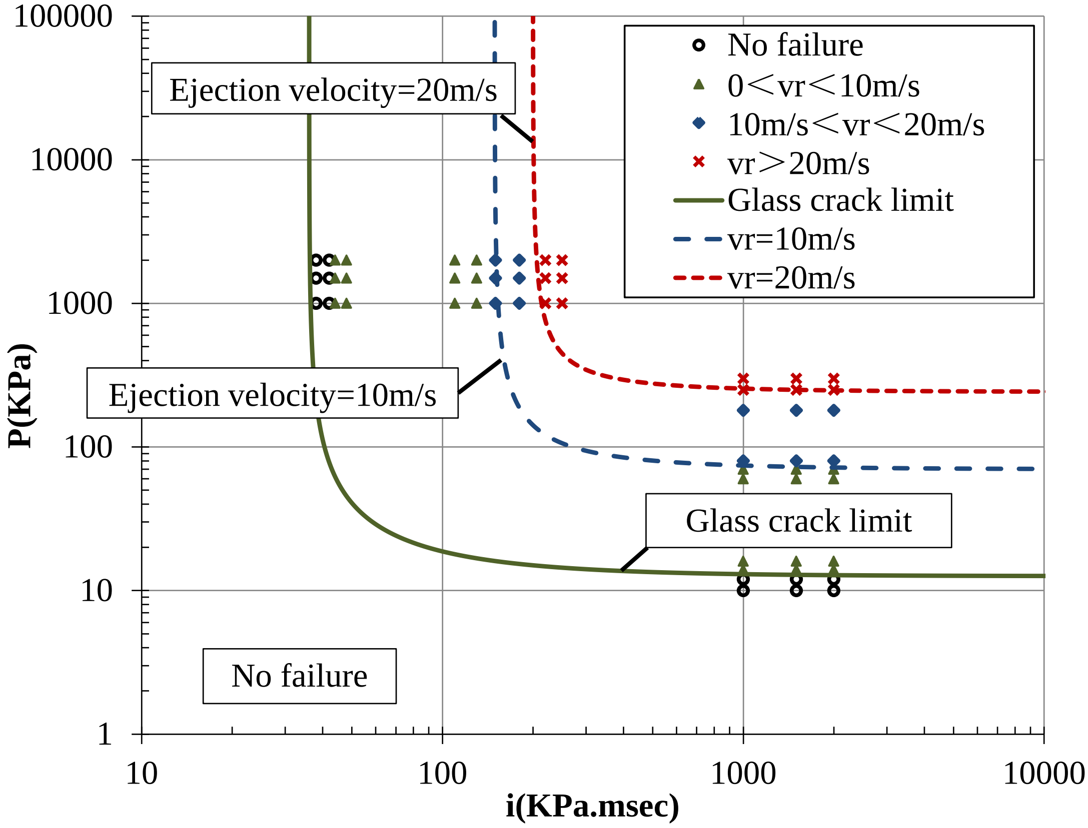


a. 1100mm×1100mm×8mm glass panel.

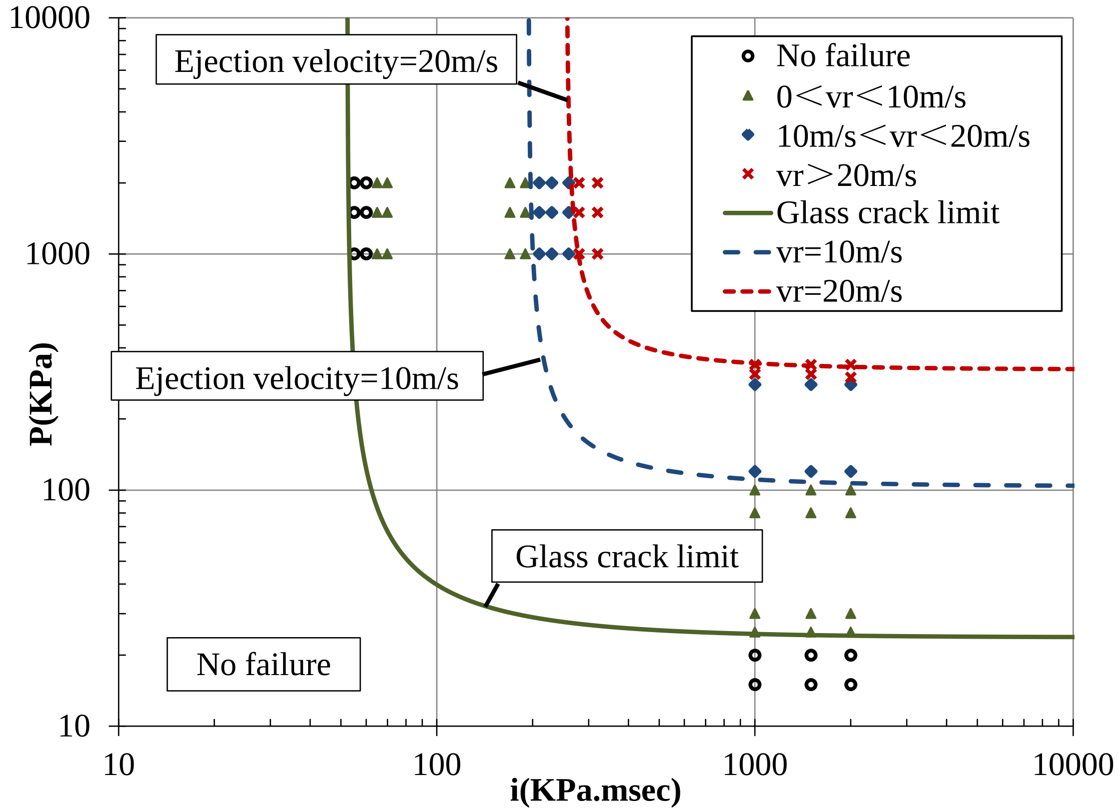

b. 1500mm×1200mm×10mm glass panel.

Figure 15. Comparison between the generated P-I curves and FEA results in impulsive and quasi-static regions

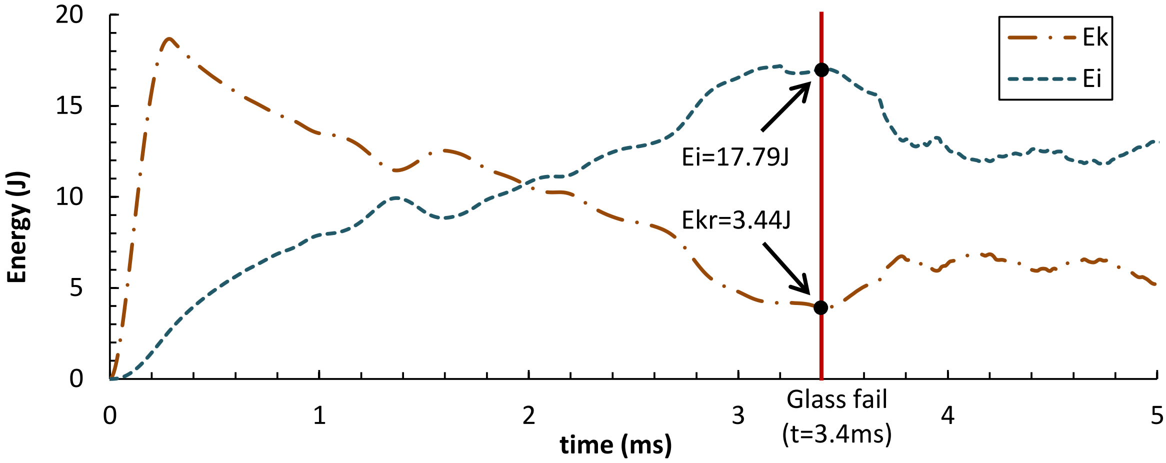


Figure 16. Time history of kinetic energy and internal energy for damage level I in impulsive asymptote, based on FE analysis

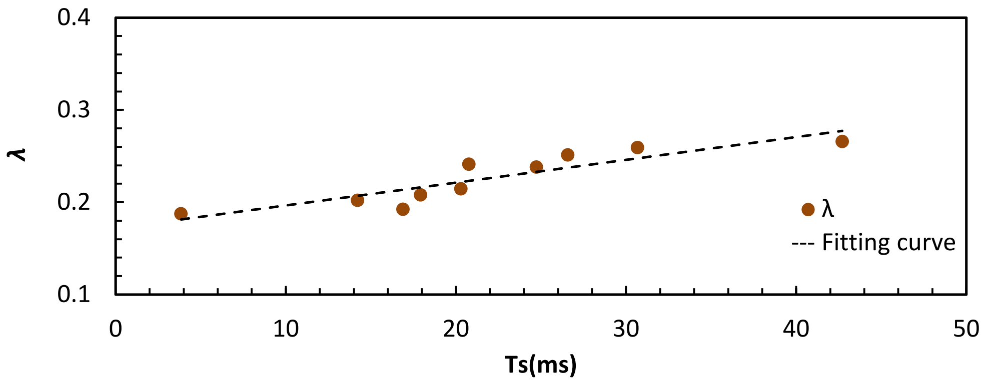


Figure 17. Incomplete conversion coefficient of kinetic energy

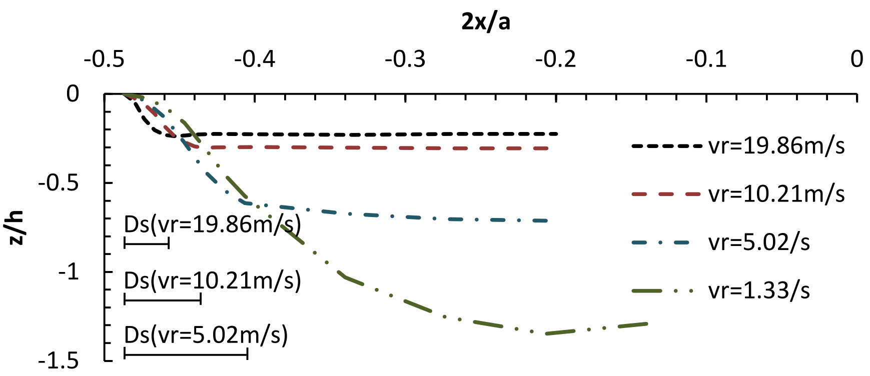


Figure 18. Deflection profiles at failure time for different ejection velocity under impulsive loading, based on FE analysis

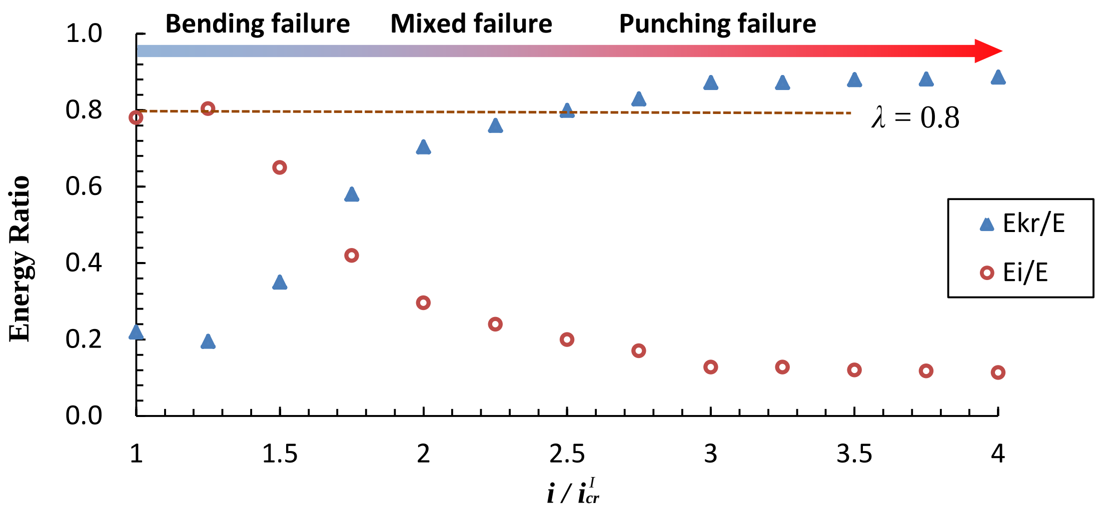


Figure 19. Relationship between energy ratio and imparted impulse